

# Chapter 1

## Introduction

The TWIST collaboration's final direct measurement of  $P_\mu^\pi \xi$  will be described, where  $P_\mu^\pi$  is the polarisation of the muon from pion decay, and  $\xi$  describes the asymmetry of the positrons from muon decay. This measurement is a high precision test of the standard model of particle physics.

The current chapter will describe the physics under investigation and previous measurements of  $P_\mu^\pi \xi$ . Chapter 2 describes the delivery of muons, the time expansion chambers that measured the muon beam, and the low mass spectrometer used to measure the positrons. Chapter 3 describes the analysis that identified particles and reconstructed their trajectories. Chapter 4 is restricted to the analysis of the time expansion chambers, and this can be skipped by a hurried reader. The detailed simulation of the particles and spectrometer is covered in Chapter 5. A subsidiary  $\mu^+$ SR experiment to determine  $P_\mu(t)$  is described in Chapter 6; this was part of the author's thesis proposal, but can be skipped since its results were uncompetitive with those from the TWIST detector. Chapter 7 describes the data accumulated in 2006 and 2007 that were analysed for this measurement. The uncertainties that dominated the  $P_\mu^\pi \xi$  measurement are described in Section 8. Lastly, the results and their physics implication are considered in Chapter 9.

Appendix A details the author's personal contributions to the experiment.

### 1.1 Standard model of particle physics

The standard model (SM) describes the fundamental particles that make up all matter, and the interactions between these particles. The model is very successful, but has known deficiencies; an extension is needed to accommodate neutrino oscillations, gravity is not included, and the fundamental interactions are not unified under a common symmetry. The model uses arbitrary parameters (masses, couplings, mixing angles, etc.) that must be measured, rather than being predicted by the SM itself[1].

In the SM, all matter is composed of fundamental spin-1/2 particles<sup>1</sup> called fermions. There are six leptons, which exist as free particles, and six quarks, which have not been

---

<sup>1</sup>Spin is an intrinsic property, such as mass or charge. More detail will be given in Section 1.2.

observed as free particles. They are grouped into three generations (I, II, III) of increasing mass scale; Table 1.1 lists the particles and their charges. The leptons are the electron ( $e^-$ ), muon ( $\mu^-$ ), and tauon ( $\tau^-$ ), all with charge ( $-e$ ), and their associated neutrinos that have no electric charge. The quark flavours are up ( $u$ ), down ( $d$ ), charm ( $c$ ), strange ( $s$ ), top ( $t$ ) and bottom ( $b$ ), and in each generation there is a quark of charge ( $+\frac{2}{3}e$ ) and ( $-\frac{1}{3}e$ ). Quarks have an extra degree of freedom, “colour charge”, which can be red, green or blue. For each fermion there is an associated anti-particle with the same mass but opposite charge and spin. Anti-particles are denoted by their opposite charge (e.g.  $\mu^+$ ) or a bar (e.g.  $\bar{\nu}_\mu$ ).

Table 1.1: Fundamental fermions in the SM, in generations of increasing mass scale[1].

Particle	Generation			$Q/ e $
	I	II	III	
leptons	$e^-$	$\mu^-$	$\tau^-$	-1
	$\nu_e$	$\nu_\mu$	$\nu_\tau$	0
quarks	$u$	$c$	$t$	+2/3
	$d$	$s$	$b$	-1/3

The SM describes three of the four fundamental interactions between fermions, which are mediated by particles of integral spin, the bosons. The strong interaction binds quarks, and is mediated by spin-1 massless gluons that also carry a colour charge; the interactions are described by quantum chromodynamics (QCD). Leptons do not carry colour, and are therefore unaffected by the strong interaction. The electromagnetic interaction is mediated by massless photon exchange, and both quarks and charged leptons can interact. The weak interaction is mediated by three massive charged bosons, the  $W^\pm$  and  $Z_0$ , each with a mass of order 100 protons. Gravity is not included in the SM, but is supposedly mediated by a spin-2 boson called the graviton. Relative to the strong interaction, the strength of the forces between two protons are  $10^{-2}$  for electromagnetic,  $10^{-7}$  for weak, and  $10^{-39}$  for gravity[1].

The charged weak interaction (WI) can convert charged leptons into neutral leptons, and vice-versa, but only within a single generation. The WI can convert quarks between generations, by defining WI eigenstates that are a mixture of mass eigenstates. The mixing is then characterised by the Cabbibo-Kobayashi-Maskawa (CKM) matrix,  $V_{\text{CKM}}$ , defined by

$$\begin{pmatrix} d' \\ s' \\ b' \end{pmatrix} = V_{\text{CKM}} \begin{pmatrix} d \\ s \\ b \end{pmatrix} = \begin{pmatrix} V_{ud} & V_{us} & V_{ub} \\ V_{cd} & V_{cs} & V_{cb} \\ V_{td} & V_{ts} & V_{tb} \end{pmatrix} \begin{pmatrix} d \\ s \\ b \end{pmatrix}, \quad (1.1)$$

where  $(d', s', b')$  are the WI eigenstates and  $(d, s, b)$  are the mass eigenstates. The elements of  $V_{\text{CKM}}$  are determined experimentally, and is found to be close to diagonal with the latest values[2]

$$V_{\text{CKM}} = \begin{pmatrix} 0.97419 \pm 0.00022 & 0.2257 \pm 0.0010 & 0.00359 \pm 0.00016 \\ 0.2256 \pm 0.0010 & 0.97334 \pm 0.00023 & 0.0415^{+0.0010}_{-0.0011} \\ 0.00874^{+0.00026}_{-0.00037} & 0.0407 \pm 0.0010 & 0.999133^{+0.000044}_{-0.000043} \end{pmatrix}, \quad (1.2)$$

under the assumption that only three generations exist.

The weak interaction was experimentally determined to not conserve parity; this is the symmetry that physical laws are the same after an improper rotation ( $\vec{r} \rightarrow -\vec{r}$ ), which is a conserved quantity under the strong and electromagnetic interactions. The operator for the weak interaction was found to be  $(V - A)$ , which resulted in maximal parity violation since this operator projects out the left-handed part of the wavefunction.  $(V - A)$  is called the SM prediction for the weak interaction since there is no experimental data to disfavour this combination of operators.

The SM includes the Glashow Weinberg Salam (GWS) model of electroweak interactions, which unifies the electromagnetic and weak interactions. At higher energies the interactions have the same strength, and symmetry is only broken at lower energies. The GWS model addresses maximal parity violation by making left-handed particles (right-handed antiparticles) transform as doublets, and the right-handed particles (left-handed particles) as singlets, so that in the first generation of fermions,

$$\begin{pmatrix} u \\ d \end{pmatrix}_L, \begin{pmatrix} \nu_e \\ e^- \end{pmatrix}_L, u_R, d_R, e_R^-. \quad (1.3)$$

The symmetries of the theory are isospin ( $I$ ) and hypercharge ( $Y$ ); the latter is defined as  $Y = Q - I_3$ , where  $Q$  is the electric charge and  $I_3$  is the third component of weak isospin. The left-handed leptons have  $I_3 = \pm\frac{1}{2}$ , and the right-handed leptons have  $I = 0$ , so that for the doublet  $Y = -\frac{1}{2}$ , and for the singlet  $Y = -1$ .

Although the SM includes the unification of the electromagnetic and weak interactions through GWS theory, it does not unify the electroweak and strong interactions. This is the subject of grand unified theories (GUTs). For more detail on the SM, the reader is referred to Refs. [1, 3], which contain explanations that are accessible to the experimentalist.

## 1.2 Spin and polarisation

Spin and polarisation are important concepts for the measurement in this thesis. The spin of a lepton is an intrinsic property, such as its mass or charge. Spin has no classical analogue, and the spin operator cannot be defined in terms of physical observables, in contrast to the orbital angular momentum operator, which is  $(\vec{r} \times \vec{p})$ . However, the spin operators do obey the same commutation relations as the orbital angular momentum, and therefore spin is considered to be an “intrinsic angular momentum”, although nothing is actually “spinning”.

Spin is quantised, and the component along a direction can only take on the values  $\hbar s_i$ , where  $s_i = -s, -s + 1, \dots, s - 1, s$  and  $\hbar s$  is the total spin. Muons are leptons, which are spin-1/2, so that the spin in a direction can be  $\pm \frac{\hbar}{2}$ .

A “spin vector” can be defined for a single particle, as the expectation of spin along each axis. This is a useful concept since the spin vector can receive a torque in a magnetic field that results in classical precession about the field direction. For an ensemble of particles with spin, the “spin polarisation” can be introduced, which describes the degree to which the spins are aligned in a particular direction. This gives a space direction about which to define a probability distribution. In this thesis, the muon (spin) polarisation is denoted  $P_\mu$ , and is always defined with respect to the magnetic field at the point of decay, which is equivalent to the  $z$ -axis in the experiment’s coordinate system.

## 1.3 Muon production

The muons in the experiment were sourced from pion decay. A high energy proton beam incident on a stationary carbon target produced  $\pi^+$ , which then decayed with a branching ratio of  $> 99.98\%$ [2] into

$$\pi^+ \rightarrow \mu^+ \nu_\mu. \quad (1.4)$$

In the  $\pi^+$  rest frame, conservation of energy and momentum leads to a  $\mu^+$  momentum,

$$p_\mu = \frac{m_\pi^2 - m_\mu^2}{2m_\pi} = 29.79 \text{ MeV}/c, \quad (1.5)$$

where the neutrino mass is assumed to be zero. The neutrino has negative helicity<sup>2</sup> (it is “left-handed”), so that its polarisation and momentum vectors are opposite[4]. The  $\pi^+$  is spin-0 and the  $\nu_\mu$  and  $\mu^+$  are spin- $\frac{1}{2}$ ; therefore conservation of angular momentum ensures

---

<sup>2</sup>The neutrino has negative chirality. Under the assumption of massless neutrinos,  $v = c$  so that the neutrino also has negative helicity.

the muon also has negative helicity, as described in Fig. 1.1.

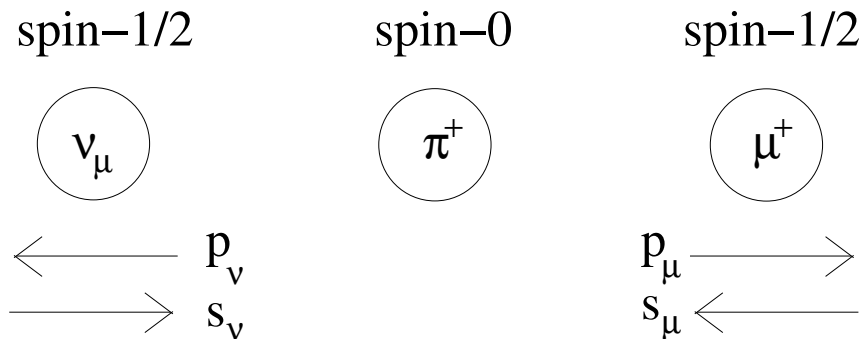


Figure 1.1: Neutrinos have their momentum ( $\vec{p}$ ) and spin ( $\vec{s}$ ) vectors in opposite directions (they are “left-handed”). Conservation of angular momentum requires the muon to also be left-handed. This is a reproduction of Fig. 1.4 from Ref. [5].

The muons from pion decay are 100% polarised, with the exception of the following mechanisms:

- Finite neutrino mass reduces the neutrino’s helicity by a factor  $(1 - p/E)$ . Even with a conservative upper mass limit<sup>3</sup> of 0.19 MeV, this changes the muon’s polarisation by just  $2 \times 10^{-5}$ , which is an order of magnitude below the experimental sensitivity<sup>4</sup>. Note that cosmological data suggests the sum of the neutrino mass eigenstates is  $< 2.0$  eV[2].
- The  $\pi^+$  has a radiative decay mode with branching ratio 0.02%,

$$\pi^+ \rightarrow \mu^+ \nu_\mu \gamma. \quad (1.6)$$

In this mode, the muon’s longitudinal polarisation is a function of photon and muon energies. The experiment selects a limited range of muon momenta, and the branching ratio for this process is already at the  $10^{-4}$  level, so the loss of polarisation due to the radiative decay mode is negligible.

<sup>3</sup>This is the 90% confidence limit from muon based neutrino mass measurements[2].

<sup>4</sup>For a finite neutrino mass, conservation of energy and momentum gives

$$E_\nu = \frac{m_\pi^2 + m_\nu^2 - m_\mu^2}{2m_\pi} = 29.79211 \text{ MeV},$$

$$p_\nu = \sqrt{E_\nu^2 - m_\nu^2} = 29.79151 \text{ MeV},$$

so that  $(1 - \beta) = 2 \times 10^{-5}$ .

- If the SM is incomplete, the weak interaction may allow for right handed neutrinos in pion decay, which would force the muon to also be right handed. The possibility of right handed muons is part of the physics motivation for measuring  $P_\mu^\pi \xi$  at the level of  $10^{-4}$  (see Section 1.5.2).

There is also a pion decay mode with branching ratio 0.0123%,  $\pi^+ \rightarrow e^+ \nu_e$ , which is observable by the experiment; see Section 2.2.5 for more details.

## 1.4 Muon decay

### 1.4.1 Decay modes

The discovery of the muon is described in Appendix B; it decays with lifetime  $2.197 \mu\text{s}$  into the three modes listed in Table 1.2, with the most probable mode shown in Fig. 1.2. The positron is emitted with a range of energies, up to a kinematic maximum of  $W_{e\mu} = (m_\mu^2 + m_e^2)/2m_\mu = 52.83 \text{ MeV}$ , which provides an energy reference feature.

Table 1.2: Muon decay modes, from the Particle Data Group[2].

Decay mode	Fraction ( $\Gamma_i/\Gamma$ )
$\mu^+ \rightarrow e^+ \nu_e \bar{\nu}_\mu$	$\approx 100\%$
$\mu^+ \rightarrow e^+ \nu_e \bar{\nu}_\mu \gamma$	$(1.4 \pm 0.4)\%$
$\mu^+ \rightarrow e^+ \nu_e \bar{\nu}_\mu e^+ e^-$	$(3.4 \pm 0.4) \times 10^{-5}$

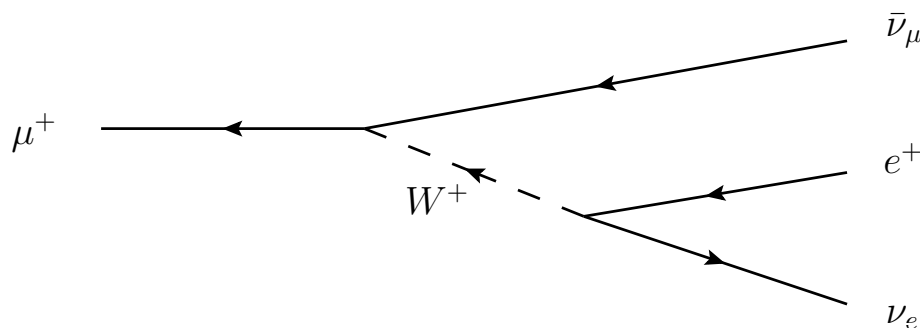


Figure 1.2: Feynman diagram for the most probable muon decay mode, produced using JaxoDraw[6].

## 1.4.2 Matrix element

The theoretical form for muon decay and the parameters that describe it are regularly reviewed by the Particle Data Group (see ‘‘Muon Decay Parameters’’ of Ref. [2]); only a summary will be included here. For energies much less than  $m_W$ , muon decay can be considered a four-fermion point interaction. The most general, local<sup>5</sup>, Lorentz-invariant, derivative-free, lepton-number-conserving matrix element  $M$  can be written in terms of helicity-preserving amplitudes as

$$M = \frac{4G_F}{\sqrt{2}} \sum_{\substack{i=L,R \\ j=L,R \\ \kappa=S,V,T}} g_{ij}^\kappa \langle \bar{\psi}_{e_i} | \Gamma^\kappa | \psi_{\nu_e} \rangle \langle \bar{\psi}_{\nu_\mu} | \Gamma_\kappa | \psi_{\mu_j} \rangle, \quad (1.7)$$

where  $G_F$  is the Fermi coupling constant ( $1.17 \times 10^{-11} \text{ MeV}^{-2}$ ),  $i$  labels the electron and muon chiralities,  $j$  labels the neutrino chiralities,  $g_{ij}^\kappa$  are complex amplitudes, and  $\Gamma^\kappa$  are the possible interactions (scalar-pseudoscalar (S), vector-axialvector (V), tensor (T)), which are given by

$$\Gamma^S = 1, \quad \Gamma^V = \gamma^\mu, \quad \Gamma^T = \frac{1}{\sqrt{2}} \sigma^{\mu\nu} \equiv \frac{i}{2\sqrt{2}} (\gamma^\mu \gamma^\nu - \gamma^\nu \gamma^\mu). \quad (1.8)$$

The amplitudes  $g_{RR}^T$  and  $g_{LL}^T$  are both zero, leaving 10 values of  $g_{ij}^\kappa$ , one of which is constrained by normalisation[8],

$$\begin{aligned} \frac{1}{4} \left( |g_{RR}^S|^2 + |g_{LR}^S|^2 + |g_{RL}^S|^2 + |g_{LL}^S|^2 \right) + |g_{RR}^V|^2 + |g_{LR}^V|^2 + |g_{RL}^V|^2 + |g_{LL}^V|^2 \\ + 3 \left( |g_{LR}^T|^2 + |g_{RL}^T|^2 \right) = 1 \end{aligned} \quad (1.9)$$

Since these are complex amplitudes, there are 18 independent parameters to determine, in addition to  $G_F$ . In the SM, where the weak vertex factor has the operator combination  $(V - A)$ , the amplitude  $g_{LL}^V = 1$  and all others are zero<sup>6</sup>.  $g_{LL}^V = 1$  is chosen since there is no experimental evidence to the contrary.

In practice, the measurements of  $g_{ij}^\kappa$  are derived from

- The muon lifetime to determine the Fermi coupling constant,  $G_F$ .

<sup>5</sup>The range of the  $W^+$  makes the interaction non-local, but this contributes a negligible deviation  $O(m_\mu^2/m_W^2)$ [7].

<sup>6</sup> $(V - A)$  corresponds to  $\gamma_\mu(1 - \gamma_5)$ . Since  $\frac{1}{2}(1 - \gamma_5)$  is the left handed chirality operator,

$$\gamma_\mu(1 - \gamma_5)|\psi\rangle = \gamma_\mu|\psi_L\rangle = \Gamma^V|\psi_L\rangle,$$

or  $g_{LL}^V = 1$ . Therefore  $(V - A)$  is the appropriate interaction when the matrix element is defined as a sum of parity eigenstates, and  $V$  for a sum over chirality eigenstates, as in Eq. (1.7).

- The energy and angle of the  $e^+$  from  $\mu^+ \rightarrow e^+ \nu_e \bar{\nu}_\mu$ , such as the experiment described in this thesis.
- The longitudinal polarisation of the  $e^+$  from  $\mu^+ \rightarrow e^+ \nu_e \bar{\nu}_\mu$ . Note this measurement also determines  $G_F$ .
- Inverse muon decay,  $\nu_\mu e \rightarrow \mu^- \nu_e$ , to place strict limits on the scalar terms.

The results from all these experiments are required to determine the  $(V - A)$  nature of the weak interaction; a global analysis is described in more detail in Ref. [7], where 11 parameters from the above experiments are used to set confidence limits on  $g_{ij}^k$ . Table 1.3 has the results from the last two global analyses, showing the impact of the TWIST experiment's published results for  $\rho$  and  $\delta$ .

Table 1.3: 90% confidence limits on the weak coupling constants. (Limits on  $|g_{LL}^S|$  and  $|g_{LL}^V|$  are from Ref. [2]). This is based on Table III from Ref. [7] and Table VI from Ref. [9].)

	Prior to TWIST[10]	First TWIST $\rho, \delta$ publication[7]	Latest TWIST results MacDonald '08[9]
$ g_{RR}^S $	< 0.066	< 0.067	< 0.062
$ g_{RR}^V $	< 0.033	< 0.034	< 0.031
$ g_{LR}^S $	< 0.125	< 0.088	< 0.074
$ g_{LR}^V $	< 0.060	< 0.036	< 0.025
$ g_{LR}^T $	< 0.036	< 0.025	< 0.021
$ g_{RL}^S $	< 0.424	< 0.417	< 0.412
$ g_{RL}^V $	< 0.110	< 0.104	< 0.104
$ g_{RL}^T $	< 0.122	< 0.104	< 0.103
$ g_{LL}^S $	< 0.550	< 0.550	< 0.550
$ g_{LL}^V $	> 0.960	> 0.960	> 0.960

### 1.4.3 Muon decay parameters

The muon decay parameters<sup>7</sup>, which describe the energy and angle of  $e^+$  from  $\mu^+ \rightarrow e^+ \nu_e \bar{\nu}_\mu$ , are defined as

$$\rho = \frac{3}{4} - \frac{3}{4} [|g_{RL}^V|^2 + |g_{LR}^V|^2 + 2 |g_{RL}^T|^2 + 2 |g_{LR}^T|^2 + \text{Re}(g_{RL}^S g_{RL}^{T*} + g_{LR}^S g_{LR}^{T*})], \quad (1.10)$$

$$\eta = \frac{1}{2} \text{Re}[g_{RR}^V g_{LL}^{S*} + g_{LL}^V g_{RR}^{S*} + g_{RL}^V (g_{LR}^{S*} + 6g_{LR}^{T*}) + g_{LR}^V (g_{RL}^{S*} + 6g_{RL}^{T*})], \quad (1.11)$$

$$\xi = 1 - \frac{1}{2} |g_{LR}^S|^2 - \frac{1}{2} |g_{RR}^S|^2 - 4 |g_{RL}^V|^2 + 2 |g_{LR}^V|^2 - 2 |g_{RR}^V|^2 + 2 |g_{LR}^T|^2 - 8 |g_{RL}^T|^2 + 4 \text{Re}(g_{LR}^S g_{LR}^{T*} - g_{RL}^S g_{RL}^{T*}), \quad (1.12)$$

$$\xi\delta = \frac{3}{4} - \frac{3}{8} |g_{RR}^S|^2 - \frac{3}{8} |g_{LR}^S|^2 - \frac{3}{2} |g_{RR}^V|^2 - \frac{3}{4} |g_{RL}^V|^2 - \frac{3}{4} |g_{LR}^V|^2 - \frac{3}{2} |g_{RL}^T|^2 - 3 |g_{LR}^T|^2 + \frac{3}{4} \text{Re}(g_{LR}^S g_{LR}^{T*} - g_{RL}^S g_{RL}^{T*}). \quad (1.13)$$

Under the SM where  $g_{ij}^k = 0$ , except for  $g_{LL}^V = 1$ , the muon decay parameters are  $\rho = \xi\delta = 3/4$ ,  $\xi = 1$  and  $\eta = 0$ . The TWIST experiment fixes  $\eta$  to the result of a global analysis, and then measures  $\rho$ ,  $\delta$  and  $P_\mu^\pi \xi$  simultaneously.

### 1.4.4 Differential decay rate

The definitions in Eqs. (1.10) to (1.13) allow a clean expression for the differential decay rate. This is proportional to  $|M|^2$ , and for a detector insensitive to the  $e^+$  polarisation is given by

$$\frac{d^2\Gamma}{dx d\cos\theta} = k(x) \{F_{IS}(x) + P_\mu \cos\theta F_{AS}(x)\}, \quad (1.14)$$

where  $x$  is the reduced energy ( $= E_e/W_{e\mu}$ ),  $\theta$  is the angle between the muon's spin and momentum vectors,  $P_\mu = |\vec{P}_\mu|$  (the degree of muon polarisation),  $k(x)$  is defined for convenience as

$$k(x) = \frac{m_\mu}{4\pi^3} W_{e\mu}^4 G_F^2 \sqrt{x^2 - x_0^2}, \quad (1.15)$$

$$W_{e\mu} = E_{\max} = \frac{m_\mu^2 + m_e^2}{2m_\mu}, \quad (1.16)$$

<sup>7</sup>These are sometimes referred to as ‘‘Michel parameters’’, after the late theoretical physicist Louis Michel, although he only introduced the  $\rho$  parameter.

and separate terms for the isotropic and anisotropic parts of the spectrum are defined,

$$F_{IS}(x) = x(1-x) + \frac{2}{9}\rho(4x^2 - 3x - x_0^2) + \eta x_0(1-x) + F_{IS}^{RC}(x), \quad (1.17)$$

$$F_{AS}(x) = \frac{1}{3}\xi\sqrt{x^2 - x_0^2} \left[ 1 - x + \frac{2}{3}\delta \left( 4x - 3 + \left( \sqrt{1 - x_0^2} - 1 \right) \right) \right] + F_{AS}^{RC}(x). \quad (1.18)$$

The superscript ‘‘RC’’ refers to radiative corrections, which are described in the next section.

### 1.4.5 Theoretical spectrum and radiative corrections

The differential decay rate is shown in Fig. 1.3, where the muon decay parameters have been set to their SM values. Radiative decays with internal and external lines are treated as spectrum corrections. These have a significant effect close to  $x = 1$ , where the rate is changed by up to 10%; the region  $x > 0.975$  is not used to extract the muon decay parameters, partly to lower the sensitivity to uncertainties in the radiative corrections. The analysis includes the following levels of correction: full first order [ $O(\alpha)$ ][11], leading-logarithmic second order [ $O(\alpha^2 L^2)$ , where  $L = \ln(m_\mu^2/m_e^2) \approx 10.7$ ][12], next-to-leading-logarithmic second order [ $O(\alpha^2 L)$ ][13, 14], and leading-logarithmic third order [ $O(\alpha^3 L^3)$ ][14]. These publications cite the TWIST experiment as significant motivation for their calculations; radiative corrections for the total decay rate calculations have been in existence for longer to help with muon lifetime measurements, but these are simpler since the electron mass can be neglected. The current analysis does not include  $O(\alpha^2 L^0)$  corrections, which became available in 2007[15];  $P_\mu^\pi \xi$  was previously found to have a negligible sensitivity to the  $O(\alpha^2 L^0)$  corrections[16].

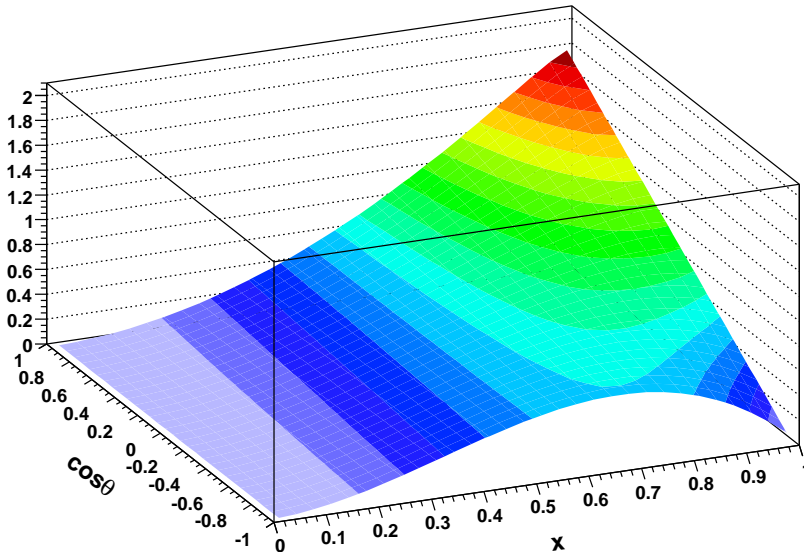
The radiative corrections assume the SM coupling for the weak interaction,  $(V - A)$ . If the muon decay parameters are found to be different from the SM values, the radiative corrections will have to be recalculated using a more general form.

The change in spectrum change due to  $P_\mu^\pi \xi$  is shown in Fig. 1.4, where the relative number of upstream and downstream counts are affected. The large  $\cos \theta$  and higher energies positrons have the most sensitivity to  $P_\mu^\pi \xi$ . TWIST simultaneously extracts  $\rho$ ,  $\delta$  and  $P_\mu^\pi \xi$ , which must satisfy  $P_\mu^\pi \xi \delta / \rho \leq 1$  to prevent an unphysical decay rate.

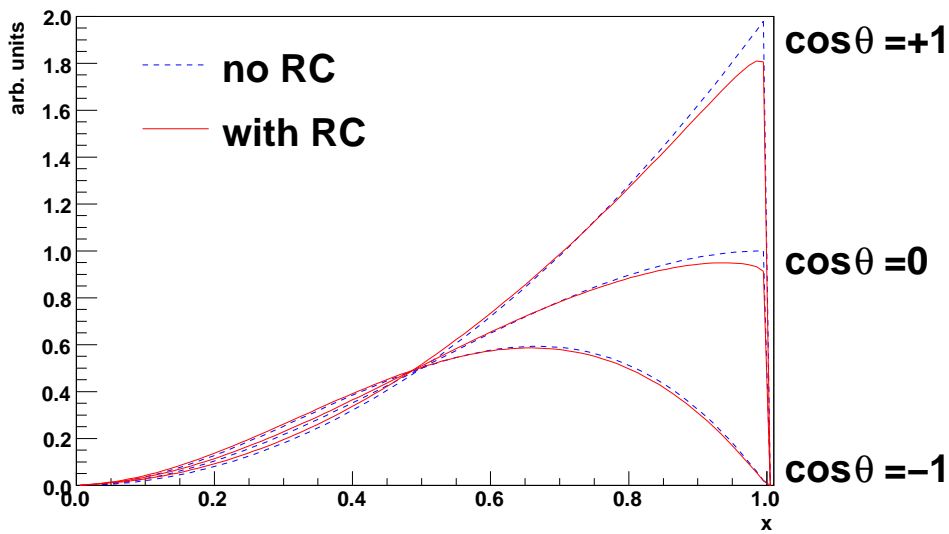
The TWIST experiment does not measure  $\eta$ , which has most sensitivity to lower energy  $e^+$ .  $\eta$  would have required  $\sim 2$  months of dedicated running with a reduced magnetic field, and careful validation of the hard scattering interactions ( $> 1$  MeV) in the simulation<sup>8</sup>. Even

---

<sup>8</sup>The hard scattering is needed since a high energy positron may experience significant energy loss in the target (a few MeV), and end up being reconstructed at a lower energy; if the simulation does not behave in



(a)  $\frac{d^2\Gamma}{dx d \cos \theta}$  from Eq. 1.14. Radiative corrections are included.



(b) Sections of Fig. 1.3(a), showing the effect of radiative corrections.

Figure 1.3: Differential decay rate for the  $e^+$  from  $\mu^+$  decay.

with these two improvements, the statistical uncertainty would have been uncompetitive with measurements derived from the  $e^+$  transverse polarisation, such as Ref. [17]. In practice, TWIST fixed  $\eta$  to the latest global analysis value of  $\eta = (-3.6 \pm 6.9) \times 10^{-3}$ [7], and included the correlation with  $\eta$  as a systematic uncertainty.

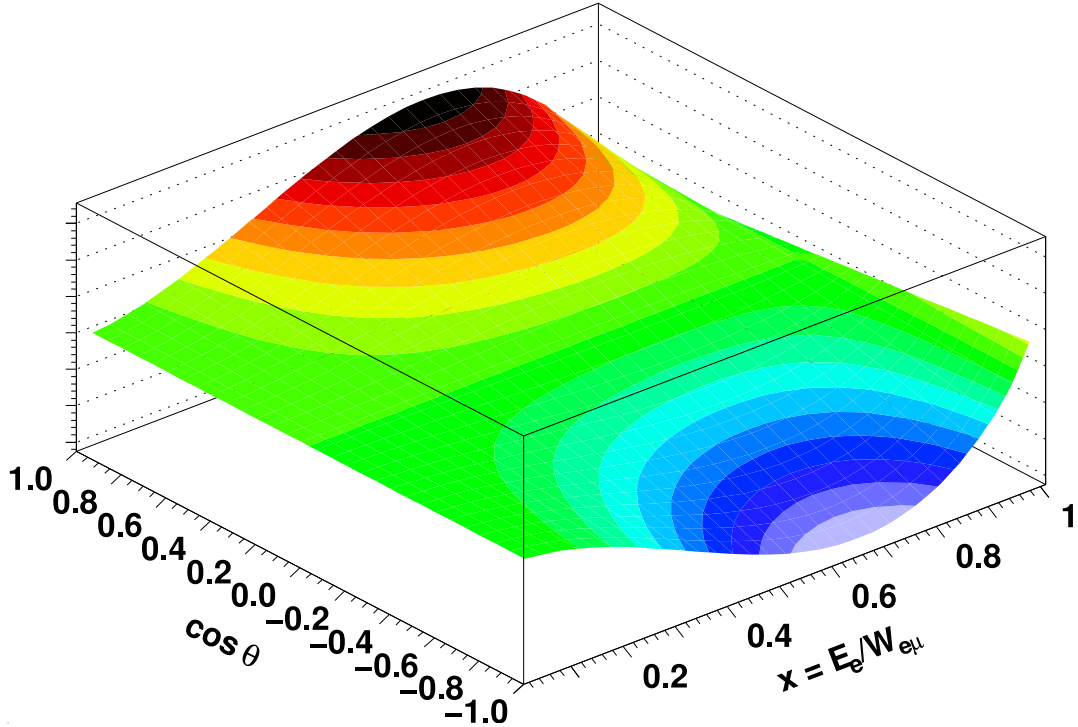


Figure 1.4: Spectrum shape of  $P_\mu^\pi \xi$ . An increase in  $P_\mu^\pi \xi$  corresponds to more counts upstream relative to downstream.

The asymmetry of the spectrum can be constructed from

$$A = \frac{N_F - N_B}{N_F + N_B}, \quad (1.19)$$

where  $N_F$  is the number of forward counts and  $N_B$  is the number of backward counts. After integration over  $x$ , this quantity depends only on  $P_\mu^\pi \xi$  and  $\eta$ , and for this reason  $P_\mu^\pi \xi$  is sometimes called the integral asymmetry parameter; see Appendix C for a detailed explanation.

---

the same way, this would result in an incorrect  $\eta$  measurement.

## 1.5 Standard Model extensions

### 1.5.1 Right handed muons

Following the notation of Eq. (1.7), the total probability for a  $j$ -handed muon to decay into an  $i$ -handed electron,  $Q_{ij}$ , can be defined as[8]

$$Q_{RR} = \frac{1}{4} |g_{RR}^S|^2 + |g_{RR}^V|^2, \quad (1.20)$$

$$Q_{LR} = \frac{1}{4} |g_{LR}^S|^2 + |g_{LR}^V|^2 + 3 |g_{LR}^T|^2, \quad (1.21)$$

$$Q_{RL} = \frac{1}{4} |g_{RL}^S|^2 + |g_{RL}^V|^2 + 3 |g_{RL}^T|^2, \quad (1.22)$$

$$Q_{LL} = \frac{1}{4} |g_{LL}^S|^2 + |g_{LL}^V|^2. \quad (1.23)$$

The coefficients on  $g_{ij}^k$  follow from the normalisation condition, Eq. (1.9). The total probability of a right-handed muon decaying into a left or right handed electron is then

$$\begin{aligned} Q_R^\mu &= Q_{RR} + Q_{LR} \\ &= \frac{1}{4} |g_{LR}^S|^2 + \frac{1}{4} |g_{RR}^S|^2 + |g_{LR}^V|^2 + |g_{RR}^V|^2 + 3 |g_{LR}^T|^2, \\ &= \frac{1}{2} \left( 1 + \frac{1}{3}\xi - \frac{16}{9}\xi\delta \right). \end{aligned} \quad (1.24)$$

where the final step used Eqs. (1.12) and (1.13).  $Q_R^\mu = 0$  for the SM values of  $\xi = 1$  and  $\xi\delta = 3/4$ . The most precise experimental values are shown in Table 9.1, where the published TWIST measurements of  $\rho$ ,  $\delta$  and  $P_\mu^\pi \xi$  have constrained  $Q_R^\mu$  by a factor of six.

Table 1.4: Probability of a right-handed muon decaying into a positron of any handedness.

Description	$Q_R^\mu$
Best result before TWIST[16].	1.4%
Global analysis using first TWIST $\rho$ , $\delta$ results[7].	0.31%
Global analysis using newest TWIST $\rho$ , $\delta$ , and $P_\mu^\pi \xi = 1.0003 \pm 0.0038$ [9].	0.23%

## 1.5.2 Left-right symmetric electroweak models

The electromagnetic and strong interactions conserve parity, yet the weak interaction has maximal parity violation ( $V - A$  currents). In left-right symmetric electroweak models (LRS models), the SM is extended by introducing a  $(V + A)$  current that couples right-handed wavefunctions, restoring parity conservation; this corresponds to  $g_{RR}^V \neq 0$  in Eq. (1.7). The  $(V + A)$  interaction is mediated by a new  $W_R$  that is much heavier than the  $W_L$ , and parity violation is a result of the mass difference between the vector bosons.

In the minimal standard model of electroweak interactions the gauge group is  $SU(2)_L \times U(1)$ . In LRS models, this is extended to  $SU(2)_L \times SU(2)_R \times U(1)$ , so that right-handed fermions also transform as doublets. The distinct vector-boson fields for the  $(V - A)$  and  $(V + A)$  currents are then mediated by a  $W_L$  and  $W_R$ , which are related to mass eigenstates  $W_1$  and  $W_2$  by

$$\begin{aligned} W_L &= W_1 \cos \zeta + W_2 \sin \zeta, \\ W_R &= e^{i\omega} (-W_1 \sin \zeta + W_2 \cos \zeta) \end{aligned} \quad (1.25)$$

where  $\zeta$  is a mixing angle, and  $\omega$  is a CP violating phase. The LRS models also introduce two additional massive neutral gauge bosons. The left and right handed interactions have separate coupling constants  $g_R$  and  $g_L$ , which correspond to  $g_{RR}^V$  and  $g_{LL}^V$  in Eq. (1.7).

The relationship between the LRS parameters and muon decay parameters has been established. Assuming that neutrinos are Dirac fermions (i.e. particle and anti-particle are different), and there is no mixing in the leptonic sector, then  $P_\mu$ ,  $\xi$ ,  $\rho$  have the relationships

$$P_\mu \simeq 1 - 2t_\theta^2 - 2\zeta_g^2 - 4t_\theta\zeta_g \cos(\alpha + \omega), \quad (1.26)$$

$$\xi \simeq 1 - 2(t^2 + \zeta_g^2), \quad (1.27)$$

$$\rho \simeq \frac{3}{4}(1 - 2\zeta_g^2), \quad (1.28)$$

where

$$t = \frac{g_R^2 m_1^2}{g_L^2 m_2^2}, \quad (1.29)$$

$$t_\theta = \frac{g_R^2 m_1^2 |V_{ud}^R|}{g_L^2 m_2^2 |V_{ud}^L|}, \quad (1.30)$$

$$\zeta_g = \frac{g_R}{g_L} \zeta, \quad (1.31)$$

$\alpha$  is a CP violating phase in the right-handed CKM matrix, and  $V_{ud}^{L,R}$  are elements of the left and right handed CKM matrices. Therefore  $P_\mu \xi$  and  $\rho$  allow limits to be set on the mass ratio,  $t$ , and the mixing angle,  $\zeta_g$ . Note that if muons are sourced from  $K^+$  decays, then the substitutions  $V_{ud}^R \rightarrow V_{us}^R$  and  $V_{ud}^L \rightarrow V_{us}^L$  must be made.

There are specific cases of LRS models that make further assumptions. In “manifest” LRS models the right- and left-handed CKM matrices are assumed to be the same,  $g_R = g_L$  and  $\omega = 0$  so that  $t_\theta = t$  and  $\alpha = 0$ . Equations (1.26) and (1.27) then reduce to

$$P_\mu \xi \approx 1 - 4t^2 - 4\zeta^2 - 4t\zeta, \quad (1.32)$$

so that

$$\zeta = \frac{1}{2} \left( -t \pm \sqrt{1 - P_\mu \xi - 3t^2} \right). \quad (1.33)$$

In pseudomanifest LRS models,  $\omega \neq 0$ , so that CP violation is still present, and

$$P_\mu \xi \approx 1 - 4t^2 - 4\zeta^2 - 4t\zeta \cos(\alpha + \omega). \quad (1.34)$$

For a more detailed discussion of the LRS models, see Ref. [18].

Direct searches for an additional heavy gauge boson have been made at the Tevatron. The most stringent lower mass limit is 1.00 TeV at 95% C.L., by the D0 collaboration[19]. These experiments must assume a manifest LRS model, and are insensitive to  $\zeta$ . The Particle Data Group regularly reviews these searches[2].

The TWIST experiment’s most precise lower mass limits are  $m_2 > 360 \text{ GeV}/c^2$  (90% C.L., manifest LRS) and  $g_L/g_R m_2 > 325 \text{ GeV}/c^2$  (90% C.L., general LRS)[20]. The TWIST best limit on the left-right mixing angle is  $|\zeta_g| < 0.022$ [9].

### 1.5.3 Supersymmetry

Supersymmetry is one proposed solution to the hierarchy problem, where the mass of the Higgs boson ( $m_H$ ) is much smaller than the Planck mass ( $\sqrt{\hbar c/G} \approx 1.2 \times 10^{19} \text{ GeV}/c^2$ ), despite the enormous one-loop corrections from every fermion that the Higgs couples to[21]. A supersymmetric boson partner is introduced for each fermion, and the boson one-loop correction then exactly cancels the fermion one-loop correction. Similarly, a supersymmetric fermion partner is introduced for each boson. The new particles required in the minimal supersymmetric standard model (MSSM) are summarised in Ref. [21]. Supersymmetry is a broken symmetry, since the partners are not observed at the same energy as the original particle, and must have much larger masses[1].

The contribution of the MSSM to muon decay has been evaluated using one loop box diagrams[22]. In the most optimistic case, the weak coupling constant  $g_{RR}^S$  is expected to have sensitivity at the 0.1% level, which is two orders of magnitude below the current experimental limit of 6% (Table 1.3). The determination of the muon lifetime (which includes  $\eta$ ) is expected to be more sensitive.

## 1.6 Muon depolarisation mechanisms

In order to measure  $P_\mu^\pi \xi$ , where  $P_\mu^\pi$  is the polarisation at the time of muon production, all sources of depolarisation must be accurately known. This section will describe processes that can change  $P_\mu$  during the muon's transport through a magnetic field and after thermalisation in a metal foil.

### 1.6.1 Depolarisation in a magnetic field

Non-relativistically, the propagation of a spin vector is governed by the equation

$$\frac{d\vec{s}}{dt} = \frac{g}{2} \frac{e}{m} (\vec{s} \times \vec{B}), \quad (1.35)$$

where  $g$  is the Landé  $g$  factor, which is measured as  $g = 2.00234$ [2]. The motion of a particle in a magnetic field is given non-relativistically as

$$\frac{d\vec{v}}{dt} = \frac{e}{m} (\vec{v} \times \vec{B}). \quad (1.36)$$

Equations (1.35) and (1.36) have precession frequencies  $\omega_p = e/m$  and  $\omega_s = eg/2m$  that differ by

$$\frac{\omega_p - \omega_s}{\omega_p} = \frac{g - 2}{2} = 1.17 \times 10^{-3}, \quad (1.37)$$

which demonstrates that if the momentum and spin vectors start anti-parallel, they will remain anti-parallel to a high degree while passing through a magnetic field.

The relativistic treatment of spin in electromagnetic fields can be found in Jackson[23], and only a summary will be presented here. The propagation is governed by the BMT (Bargmann, Michel, Telegdi) equation[24],

$$\frac{dS^\alpha}{d\tau} = \frac{e}{mc} \left[ \frac{g}{2} F^{\alpha\beta} S_\beta + \frac{1}{c^2} \left( \frac{g}{2} - 1 \right) U^\alpha (S_\lambda F^{\lambda\mu} U_\mu) \right], \quad (1.38)$$

where  $S^\alpha$  is the particle's spin 4-vector,  $\tau$  is the proper time,  $F^{\alpha\beta}$  is the electromagnetic field and  $U^\alpha$  is the 4-velocity. Jackson manipulates this expression into the Thomas equation,

$$\frac{d\vec{s}}{dt} = \frac{e}{mc} \vec{s} \times \left[ \left( \frac{g}{2} - 1 + \frac{1}{\gamma} \right) \vec{B} - \left( \frac{g}{2} - 1 \right) \frac{\gamma}{\gamma + 1} (\vec{\beta} \cdot \vec{B}) \vec{\beta} - \left( \frac{g}{2} - \frac{\gamma}{\gamma + 1} \right) \vec{\beta} \times \vec{E} \right], \quad (1.39)$$

which is the form used to simulate the spin in Section 5.7. There are theoretical limitations to Eq. (1.38), since it is derived for spatially homogeneous electromagnetic fields, and can only be used in inhomogeneous situations when the field gradients are “sufficiently small and the relevant effects are of first order in the spin variable” [25]. Pierre Depommier determined that such inhomogeneous effects are completely negligible ( $\sim 10^{-12}$ ) for TWIST[26]. In addition, quantum mechanical contributions are negligible since the magnetic field does not change on a distance scale comparable to the de Broglie and Compton wavelengths of the muon.

## 1.6.2 Depolarisation while slowing down

When a muon encounters material, there is an electric field between the nucleus and atomic electrons, which is Lorentz transformed to a magnetic field in the muon's rest frame. This magnetic field rotates the polarisation vector, and for muons with momentum 29.6 MeV/c that entirely slow down in aluminium, the resulting depolarisation is  $\approx 4 \times 10^{-5}$ , (negligible)[27].

Inside material the muon is multiple scattered, which changes the momentum vector but not the polarisation vector. This changes their relative orientation, but is not a depolarisation for TWIST, since the polarisation is unchanged relative to a fixed axis.

As the muon velocity becomes comparable to the atomic electron velocity, the time between collisions is reduced, and electron capture and subsequent electron loss can repeatedly

take place. The muon forms Muonium ( $\mu^+e^-$ )<sup>9</sup>, which is a hydrogen-like state that depolarises due to the hyperfine interaction between the muon and electron spins (there is a transfer of the muon’s spin to the electron)[29]. This only becomes important at a few keV, and does not occur in metals since the conduction electron concentration effectively screens the muon from interactions with individual electrons[30]. The experiment carefully selects muons that stop inside a metal target, so that depolarisation from Muonium formation is not a concern.

Finally, there is depolarisation due to muon-electron scattering. This has been calculated for 29.6 MeV/c muons[30, 31], and is at the level of  $1 \times 10^{-5}$  (negligible).

### 1.6.3 Depolarisation after thermalisation

Muons were stopped in aluminium and silver foils of purity  $> 99.999\%$ , immersed in a 2.0 T longitudinal magnetic field. After motional thermalisation, the muons can be depolarised by nuclear dipole moments, conduction electrons, and paramagnetic impurities. The form of the resulting depolarisation has been studied by the condensed matter community using the  $\mu^+$ SR technique[32]. However, depolarisation under the TWIST conditions (strong longitudinal field, high purity metal, room temperature) is challenging to measure since it’s often considered to be negligible.

The behaviour of the muon after motional thermalisation and the available depolarisation mechanisms will now be described in more detail.

#### Muon motion

The muon is positively charged, limiting its instantaneous position to interstitial sites (i.e. between nuclei), or substitutional sites, (i.e. “vacancies”, where a nucleus is absent from the lattice). When nearly thermalised, the muons acquire electrons to lower their energy, attracting a screening charge of conduction electrons[33]. After motional thermalisation, room temperature ensures the muons are not stationary, and instead “hop” between energetically allowed sites before decaying. The conduction electrons in aluminium and silver efficiently screen the ionic potentials, allowing for high mobility[34], even over macroscopic distances of  $\lesssim 1 \mu\text{m}$ [35]. An individual muon can therefore sample a significant amount of the target before decaying.

---

<sup>9</sup>The “onium” suffix is usually reserved for bound states of a particle and its antiparticle, such as positronium, pionium and quarkonium. Therefore the assignment of “muonium” to the state  $\mu^+e^-$  is not strictly correct, and means that the bound state  $\mu^+\mu^-$  is referred to as the “bound muon-antimuon state”. After more than two decades of widespread usage, the name “muonium” for  $\mu^+e^-$  was eventually recommended by the International Union of Pure and Applied Chemistry (IUPAC)[28] in 2001.

Defects can form in the manufacturing process, such as when an aluminium sheet is cold-rolled to produce a thin foil, and this can limit the muon mobility with a strong sample dependence[35]. Defects can be removed by annealing, where the metal is maintained close to melting point for several hours and then slowly cooled. Defects can be enhanced by quenching, where the sample is rapidly cooled. Samples of 99.9995% pure aluminium that were annealed and quenched have been compared over a temperature range of 19 K to 900 K[36], and most defects were found to be absent after allowing the quenched sample to reach room temperature. The TWIST targets were supposed to be annealed by the manufacturer.

Thermalisation of the muon can result in lattice defects. The muon imparts recoil energy to the lattice on a time scale  $10^{-17}$  s, and the lattice distributes energy to neighbouring atoms in about  $\sim 10^{-12}$  s[37]. The nucleus can be knocked out of its lattice position and into an interstitial site, leaving a vacancy (a “Frenkel pair”). These vacancies are unstable, and are eliminated in  $\sim 10^{-11}$  s[37]. In other words, the lattice damage due to the muon is healed after tens of picoseconds, and in general radiation damage is hard to induce in metals[38] Reference [37] confirms that aluminium undergoes complete recovery from radiation damage for a temperature range  $200 \text{ K} < T < 300 \text{ K}$ . In addition, the location of thermalisation is expected to be of order  $1 \mu\text{m}$  from the last defect introduced[33]. Brice[39] carried out calculations that included aluminium, finding the separation is “several thousand Ångstroms ... Thus, vacancies produced by the implantation will have no significant effect on the room temperature muon diffusion rate over its lifetime”.

### Nuclear dipole moments

The evidence for rapid diffusion in metals comes from measurements of the nuclear dipole moments. Magnetic fields from the nuclei and lattice impurities can be modelled as static, isotropic and Gaussian[40] (the “Van Vleck limit”), and for diffusing particles the depolarisation is then given by[41],

$$P(t) = P(0) \exp \left\{ -\frac{2\Delta^2}{\nu^2} [\exp(-\nu t) - 1 + \nu t] \right\}, \quad (1.40)$$

where  $\Delta/\gamma_\mu$  is the variance of the field distribution<sup>10</sup> and  $1/\nu$  is the mean time between a hop. If an external field  $B_{\text{ext}}$  is now applied in a direction *transverse* to the muon polarisation,

---

<sup>10</sup>In the Van Vleck limit, the field distribution is modelled by  $D(B_{\text{local}}) \sim \exp \left[ -\frac{B_{\text{local}}^2}{2\Delta^2/\gamma_\mu} \right]$ , so that  $\Delta/\gamma_\mu$  is the variance.

the muon spins precess and are depolarised according to the Abragam formula<sup>11</sup>,

$$P(t) = P(0) \exp \left\{ -\frac{\Delta^2}{\nu^2} [\exp(-\nu t) - 1 + \nu t] \right\} \cos(\omega_\mu t), \quad (1.41)$$

where  $\omega_\mu = \gamma_\mu B_{\text{ext}}$ . In the motional narrowing limit, the muons move quickly so that  $\nu$  is large,  $\exp(-\nu t) \rightarrow 0$ , and the envelope of Eq. (1.41) limits to an exponential time dependence. In the static limit, the envelope limits to a Gaussian time dependence. If a *longitudinal* field  $B_0$  is applied instead, the relaxation rate becomes[43],

$$P(t) = 1 - \frac{2\Delta^2}{\omega_0^2} [1 - \exp(-\frac{1}{2}\Delta^2 t^2) \cos \omega_0 t] + \frac{2\Delta^4}{\omega_0^3} \int_0^t \exp\left(-\frac{1}{2}\Delta^2 \tau^2\right) \sin \omega_0 \tau d\tau, \quad (1.42)$$

where  $\omega_0 = \gamma_\mu B_0$ , and the longitudinal field is seen to suppresses the depolarisation due to nuclear dipole moments. The largest observed field on a muon in a crystal cell is  $\Delta/\gamma_\mu = 4.7 \text{ G}$ [41], and the field at the metal target in TWIST is longitudinal with  $B_0 = (20 \times 10^3) \text{ G}$ , so that  $(2\Delta^2/\omega_0^2) < 10^{-7}$ . Depolarisation by nuclear dipole moments is therefore negligible for TWIST.

$\mu^+$ SR experiments have measured depolarisation in aluminium and silver due to nuclear dipole moments, using a transverse magnetic field arrangement. There are more studies on aluminium since its nuclear dipole moment is about 35 times larger than silver. Even with its large dipole moment, high purity aluminium leads to almost negligible depolarisation down to 1 K[44, 45, 46, 47, 48]. As a result, experimenters have to dope the sample with impurities to actually measure depolarisation[33, 49, 50].

There is a contradictory measurement in Ref. [51], which uses 99.99% pure aluminium and silver targets in a transverse field arrangement at room temperature, and observe a Gaussian form for the depolarisation. Their sample was a foil, which may have defects originating from the cold-rolling during manufacture. Note that a later publication by the same group used a longitudinal field, and finds no clear evidence of depolarisation, as expected from Eq. (1.42).

## Korringa relaxation

A hyperfine contact interaction between the muon spin and the conduction electron spin can lead to a depolarisation. The theory for such an interaction was originally treated in the

---

<sup>11</sup>See p439 of Ref. [42]. Note this is also called the Anderson form, and the Kubo-Tomita form.

context of NMR<sup>12</sup> by Korringa[52], and is therefore named “Korringa relaxation”. A modern derivation in the context of muons has been carried out[53]. The muon attracts electrons which enhance the local spin density. Paraphrasing the descriptions in Refs. [53, 54], the conduction electrons then hop on and off the muon, making the net hyperfine coupling experienced an average of the electron spin orientations. A simultaneous flip of the electron and muon spins can take place, with the energy provided by a change in the electron’s kinetic energy[42]. The participating electrons are within  $kT$  of the Fermi surface, from which Ref. [53] derives,  $\lambda \propto T$ . The signature of the Korringa relaxation is an increase in rate with temperature, and an insensitivity of rate to applied magnetic field.

Conduction electron depolarisation is often considered “unobservably slow”[53]. Reference [55] was surprised to find measurable longitudinal depolarisation in several non-magnetic metals (lead, cadmium, zinc, copper); unfortunately they did not examine aluminium and silver. They found the relaxation rate increased with temperature, and was robust to field changes in the range 0.010 T to 0.200 T, which is evidence of Korringa relaxation.

## Impurities

This aluminium stopping target was purchased from Goodfellow, who gave the typical impurities as Cu 0.3 ppm<sup>13</sup>, Fe 0.3 ppm, Mg 1.2 ppm, and Si 0.8 ppm. The silver stopping target was purchased from ESPI, who gave the typical impurities as Fe 2 ppm, Bi < 2 ppm, Cu 0.6 ppm, and Pd 0.6 ppm. The impurities take the place of an aluminium or silver nucleus, and can only trap muons below temperatures of  $\approx 20$  K[48]. The non-paramagnetic ions can depolarise muons due to their nuclear dipole moments, using the arguments from Section 1.6.3. Paramagnetic ions (Fe in this case) are a concern since they can depolarise due to their electronic dipole moment, which is much larger than the nuclear dipole moment[56], producing fields as large as 1 kG at a distance of one lattice spacing[5]. The depolarisation form in this case is exponential[42, 56].

---

<sup>12</sup>In NMR spectroscopy, a substance is immersed in a static magnetic field and then exposed to electromagnetic (EM) radiation. For the nuclei in the substance that have intrinsic magnetic moments (those with an odd number of protons or neutrons), the static magnetic field creates an energy difference between the spin states. The frequency of the EM radiation is swept, and peak absorption will occur (“resonance”) when the energy of the photons matches the energy difference between the spin states.

<sup>13</sup>ppm = parts per million. A concentration of 1 ppm corresponds to one impurity for every 100 crystal cells.

## Summary

Relaxation due to nuclear dipole moments, whether they come from the metal nuclei or non-paramagnetic impurities, is heavily suppressed by the presence of a longitudinal field. Even if there were contributions from nuclear dipole moments, the muons are expected to be in rapid motion, for which the appropriate form is exponential. Later it will be shown the measured relaxation rates for silver and aluminium differ by a factor of two, yet the nuclear dipole moments differ by a factor of 35, providing further evidence that the depolarisation is not from nuclear dipole moments. Paramagnetic impurities would also cause exponential relaxation. The TWIST samples are annealed, which makes trapping at defects unlikely. Even if muons did trap at defects or vacancies, the longitudinal field holds their spin against depolarisation by nuclear dipole moments. The most likely cause of depolarisation is Korringa relaxation, which has been observed in other metals, and has an exponential form.

## 1.7 Previous $P_{\mu}^{\pi} \xi$ measurements

In 1956, Lee and Yang observed that parity is conserved in strong and weak interactions, but in weak interactions “is so far only an extrapolated hypothesis unsupported by experimental evidence” [57]. They suggested several experiments to investigate parity conservation in the weak interaction, including the asymmetry of muon decay.

The angular distribution of decay positrons will generally follow a distribution  $(1+a \cos \theta)$ . For  $\eta = 0$ ,  $a = P_{\mu}^D \xi / 3$ , where  $\xi$  is the intrinsic asymmetry parameter, and  $P_{\mu}^D$  is the polarisation of the muon at the moment of decay. The polarisation at the time of muon production can only be inferred if all sources of depolarisation are evaluated.  $a = 0$  implies that parity is conserved, and  $P_{\mu} \xi = \pm 1$  implies maximal violation of parity.

Two classes of asymmetry measurements will now be described:  $P_{\mu}^{\pi} \xi$  and  $P_{\mu}^K \xi$ , where muons are sourced from pion and kaon decay respectively. The results are interpreted differently in the context of LRS models (see Eqs. (1.26) to (1.31) and surrounding text). In addition,  $\tau$  decay experiments have confirmed  $P_{\mu}^{\tau} \xi$  is consistent with 1.0 using the modes  $\tau^{\pm} \rightarrow \mu^{\pm} \nu \bar{\nu}$  and  $\tau^{\pm} \rightarrow e^{\pm} \nu \bar{\nu}$ , but these measurements had uncertainties greater than 10% [58, 59, 60];  $\tau$  decay experiments are more useful as a check on lepton universality, rather than a precision asymmetry measurement.

### 1.7.1 Measurements of $P_\mu^\pi \xi$

A year after Lee and Yang's publication, positive muons from pion decay were stopped in carbon, and the angular distribution of decay positrons was found to follow  $(1 + a \cos \theta)$ , and “ $a = -\frac{1}{3}$  with an estimated error of 10%” [61]. Assuming no depolarisation took place while slowing down, stopping, and during the  $1 \mu\text{s}$  the muon spent in the carbon target, this result suggested  $P_\mu \xi = 1.0 \pm 0.1$ , which was consistent with maximal parity violation.

Over the next three years (1957 to 1960) many similar experiments took place [62]. A popular technique was to stop a beam of pions in nuclear emulsion<sup>14</sup>; this had the advantage of delivering muons with full polarisation, but the disadvantages of low statistics and poorly determined depolarisation within the emulsion itself due to Muonium formation. This depolarisation was found to depend on the applied magnetic field, yielding values of  $P_\mu \xi$  in the range  $0.33 \pm 0.03$  (zero field) to  $0.97 \pm 0.06$  (2.7 T) [63]; see Ref. [62] for the intermediate field results.

The other techniques used muon beams that were stopped in a variety of targets. There were challenges in producing a muon beam with high polarisation; in early attempts, a production target was placed within the cyclotron, but this produced a muon beam with poorly determined polarisation. Later the technique of surface muon beams was developed, which is described later in Section 2.2.2. The Bardon, Berley and Lederman experiment [64] instead used a  $\pi^+$  beam that decayed in flight, to produce a highly transverse polarised  $\mu^+$  beam at the jacobian angle. The  $\mu^+$  were stopped in a bromoform target, which had small but unknown depolarising effects; in consequence, the experiment's result was a lower limit. Depolarisation from magnetic fields was eliminated by using Helmholtz coils to cancel the cyclotron's field. Decay positrons were detected with opposing counters. A solenoid surrounding the target rotated the muon spin  $\pm 90^\circ$ , allowing the  $e^+$  distribution to be turned around in one hour cycles. The experiment found  $|\xi| \geq 0.97 \pm 0.05$ .

Muons were also stopped in liquid hydrogen, in bubble chamber experiments. The particles leave ionisation tracks that are curved by a magnetic field to determine momentum. The most accurate experiment was carried out by Plano, who measured  $P_\mu \xi$ ,  $\delta$  and  $\rho$ , and found  $|\xi| = 0.94 \pm 0.07$  [65].

There was apparently no improvement in direct measurements until 1967, when a nuclear emulsion experiment determined  $P_\mu \xi = 0.975 \pm 0.015$ , which is  $1.7\sigma$  from the (V-A) prediction [66]. The depolarisation within the emulsion may have been underestimated [62, 67].

Prior to the TWIST experiment, Beltrami had the most precise direct measurement

---

<sup>14</sup>A photographic plate is exposed to particles and later developed. The emulsion is predominantly silver promide by weight, but by number of atoms, it's 25% silver bromide, 75% gelatin [62].

of  $P_\mu^\pi \xi$ [67]. A 150 MeV/c  $\pi^+$  beam decayed in flight, and a transversely polarised muon beam was extracted close to the jacobian angle; this is the same approach taken by Bardon experiment[64] described above. The muons were moderated by aluminium and stopped in a Beryllium (Be) target. The  $\mu^+$ SR technique was then used to measure the decay  $e^+$  asymmetry, with the muon spins precessed by a 3 mT field. A pure exponential depolarisation form for  $P_\mu(t)$  was assumed in the Be. The experiment did not measure the decay  $e^+$  momentum, so there was no magnetic field requirement, and hence no associated systematic uncertainty. The contribution from muons stopping in a trigger scintillator immediately before the Be target was measured by removing the target, and found to be negligible ( $2 \times 10^{-3}$  per event). The final result was  $1.0027 \pm 0.0079$  (stat.)  $\pm 0.0030$  (syst.).

The most precise direct measurement is  $P_\mu^\pi \xi = 1.0003 \pm 0.0006$  (stat.)  $\pm 0.0038$  (syst.), published by the TWIST experiment in 2006[5, 20]. The leading term in the systematic uncertainty was  $33 \times 10^{-4}$ , due to limitations in the reproducibility of the muon beam's initial position and angle; the current thesis aims to reduce this uncertainty by improving the knowledge of the muon beam and solenoidal magnetic field through which the beam passes.

Figure 1.5 summarises the *direct* measurements that have been described so far. All are seen to be consistent with  $P_\mu \xi = 1$ . Additional *indirect* measurements are possible, using the result  $P_\mu \xi \delta / \rho > 0.99682$  (90% confidence)[30, 31]; in this experiment the region of the spectrum with  $x > 0.97$  was measured, using the same beam line as the TWIST experiment. Muons were stopped in several targets, including silver and aluminium with the same purity as TWIST. The confidence interval can be combined with the latest  $\rho$  and  $\delta$  measurements to determine  $0.99524 < P_\mu^\pi \xi \leq \xi < 1.00091$  (90% confidence)[9].

### 1.7.2 Measurements of $P_\mu^K \xi$

The first measurement of  $P_\mu^K \xi$  with an uncertainty below 10% is described in Refs. [68, 70]. (There were three prior experiments that were consistent with  $P_\mu^K \xi = 1$ , but with uncertainties  $> 10\%$ [71, 72, 73].) A 236 MeV/c muon beam was sourced from stationary  $K^+$  decays via the mode  $K^+ \rightarrow \mu^+ \nu$ . The  $\mu^+$  were degraded by carbon, and stopped in a 99.99% aluminium target. The muon trajectory immediately before the target was measured using a pair of orthogonal multiwire proportional chambers (MWPCs), which established the muon spin, and the decay positrons were measured with a different pair of MWPCs. A transverse magnetic field was applied to precess the muon spin, and the asymmetry's dependence on time was fit to determine  $P_\mu^K \xi = 0.970 \pm 0.047$  (stat.)  $\pm 0.005$  (syst.), under the assumption of no depolarisation while slowing down, and within the aluminium target;

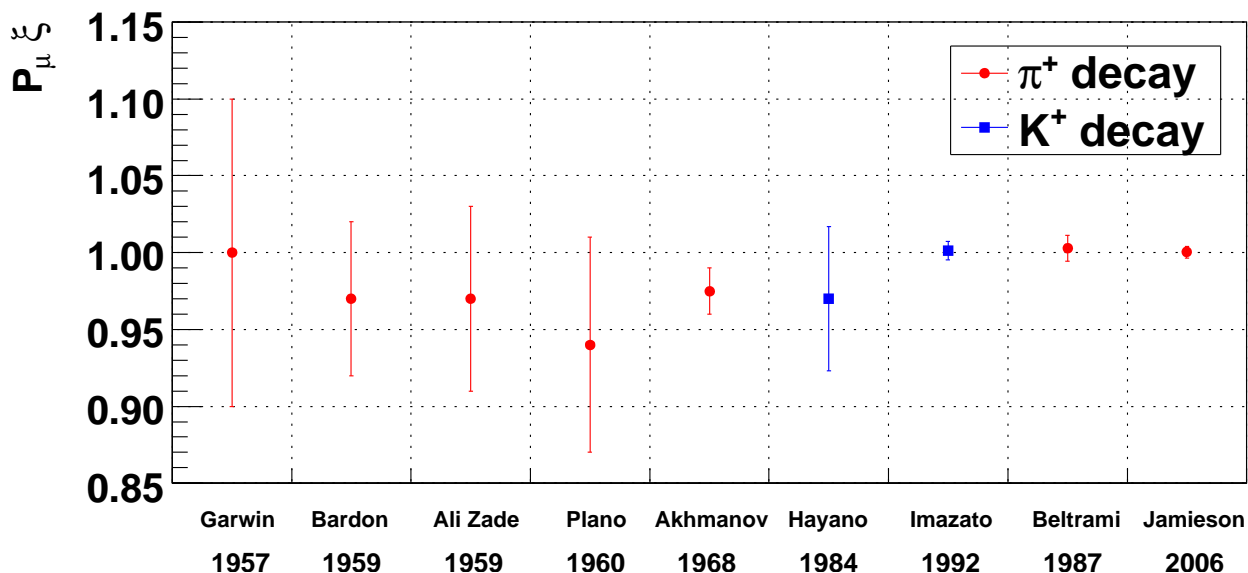


Figure 1.5: Previous direct measurements of  $P_\mu \xi$  with uncertainties less than 10%. The statistical and systematic uncertainties have been added in quadrature. Measurements are from Refs [20, 61, 63, 64, 65, 66, 67, 68, 69].

these are safe assumptions at the few percent level of precision. The measurement was limited by statistical uncertainty.

A more precise measurement using a similar technique is described in Ref. [69]. The muon source was the same, but with higher flux, and the muons were again degraded by carbon and stopped in high purity aluminium ( $> 99.999\%$  in this case). The incident muon was measured more carefully to determine its spin, using four  $x$  and  $y$  layers of drift chambers before the carbon degrader, and two MWPCs after the degrader and before the aluminium stopping target. The decay positrons were measured using two arms, each with four horizontal and four vertical drift chambers. A transverse magnetic field precessed the muon's spin. The polarisation was allowed to relax in the aluminium target, but the form for  $P_\mu(t)$  was not stated. The final result was  $P_\mu^K \xi = 1.0013 \pm 0.0030$  (stat.)  $\pm 0.0053$  (syst.), where the leading systematic uncertainty was from a correction due to knock-on electron production in the stopping target.

# Appendix B

## History of the muon

In 1935, Yukawa postulated the existence of a new field to explain the binding between nucleons[102], with the force mediated by a heavy quantum. The electromagnetic field was already known to mediate force with its own light quantum, namely the photon. Yukawa predicted the nuclear force quantum would have unit charge, mass “ $2 \times 10^2$  times as large as the electron”, and substantial interactions with matter. The new field would be very strong, but only over a small range due to the quantum’s mass.

In 1936, Anderson and Neddermeyer published cloud chamber observations of cosmic rays[103], and noted “About one percent of the exposures ... reveal the presence of strongly ionizing particles which in most cases seem to be protons ... and usually arise from a type of nuclear disintegration not heretofore observed.” In the years following this publication, the authors and other independent experimenters published new results on these particles, with the mass “ranging from 120 to about 400 electron masses”[104], “about 240 electron-masses”[104] and eventually “in the neighbourhood of 200 electron masses”[105]. Many people believed that Yukawa’s postulated particle had been discovered.

World War II interrupted pure physics research. Shortly after the war, physicists were keen to understand the muon better, and identify whether it was really the Yukawa particle. The particle appeared to have the correct charge and mass, but Yukawa had predicted a particle that interacted strongly with matter, with “its flight halting abruptly the very moment it passed an atomic nucleus”[106]. In 1946, Conversi, Pancini and Piccioni demonstrated that positive and negative muons stopping in graphite produced a similar number of decay electrons[107], in contrast to the theoretical prediction that negative muons should produce far less decay electrons due to nuclear capture. Fermi, Teller and Weisskopf subsequently concluded “the interaction of mesotrons with nucleons according to the conventional schemes is many orders of magnitude weaker than usually assumed”[108]. The muon no longer appeared to be the Yukawa particle.

The issue was resolved when Powell’s collaboration discovered the real Yukawa particle, the pion[109, 110]. They observed “two types of mesons exist, of different mass, which we refer to as  $\pi^-$  and  $\mu^-$  mesons”[110]. The pion was short lived and therefore had been harder to detect. The discovery of the pion meant the muon was not predicted at all, leading the

theorist I.I. Rabi to famously exclaim "Who ordered that?" [57]. The mass of the muon is now determined as 105.7MeV (211 electron masses), and the charged pions have mass 139.6MeV (280 electron masses). The true carriers of the strong force are also identified as gluons, not the pion.

Detailed accounts of the muon's history can be found in Refs. [3, 106, 111, 112]. The very early history is well summarised in Ref. [105].

# Appendix C

## Asymmetry

This section is a summary of private communication between the author and C. Gagliardi (Texas A&M University).

The term ‘‘asymmetry’’ and its connection to  $P_\mu^\pi \xi$  must be carefully defined. In general the asymmetry,  $A$ , is given by

$$A = \frac{N_F - N_B}{N_F + N_B}, \quad (\text{C.1})$$

where  $N_F$  is the number of forward counts and  $N_B$  is the number of backward counts. For a detector with angular fiducial ( $a < \cos \theta < b$ ) in the forward (upstream) direction, and a symmetric fiducial of  $[(-b) < \cos \theta < (-a)]$  in the backward (downstream) direction, Eqs. (1.14)-(1.18) predict the number of forward and backward counts as

$$\begin{aligned} N_F(x) &= \int_a^b \left( \frac{d^2\Gamma}{dx d\cos\theta} \right) d\cos\theta \\ &= k(x) \left[ F_{IS}(x)(b-a) + \frac{1}{2}(b^2 - a^2)P_\mu F_{AS}(x) \right], \end{aligned} \quad (\text{C.2})$$

$$N_B(x) = k(x) \left[ F_{IS}(x)(b-a) - \frac{1}{2}(b^2 - a^2)P_\mu F_{AS}(x) \right]. \quad (\text{C.3})$$

$N_F(x)$  and  $N_B(x)$  both separately depend on all four muon decay parameters, and could be fit separately to extract results. However, in practice the increased correlations make this undesirable. Neglecting radiative corrections, the rate for the total number of counts at each  $x$  (‘‘sum’’) and the rate for the forward-backward difference (‘‘diff’’) can be evaluated as

$$\begin{aligned} \text{sum} &= N_F + N_B = 2k(x)(b-a)F_{IS} \\ &= 2k_0(b-a)\sqrt{x^2 - x_0^2} \times \\ &\quad \left[ \left( \frac{8}{9}\rho - 1 \right) x^2 + \left( 1 - \frac{2}{3}\rho - \eta x_0 \right) x + \left( \eta x_0 - \frac{2}{9}\rho x_0^2 \right) \right], \end{aligned} \quad (\text{C.4})$$

and

$$\begin{aligned}
 \text{diff} &= N_F - N_B = (b^2 - a^2)k(x)P_\mu F_{AS} \\
 &= 2k_0(b^2 - a^2) [P_\mu \xi] (x^2 - x_0^2) \times \\
 &\quad \left[ \left( \frac{8}{3}\delta - 1 \right) x + \left( 1 - 2\delta + \frac{2}{3}\delta \left( \sqrt{1 - x_0^2} - 1 \right) \right) \right]. \tag{C.5}
 \end{aligned}$$

Therefore a fit of “sum” against  $x$  can determine  $\rho$  and  $\eta$ , and a fit of “diff” against  $x$  can determine  $\delta$ . The quantity “diff” is equal to  $P_\mu^\pi \xi$  multiplied by a rate, meaning that a large  $P_\mu^\pi \xi$  and a small total number of events looks the same, and vice-versa. As a result, it’s impossible to extract  $P_\mu^\pi \xi$  from the difference alone.

Now consider the asymmetry, defined in Eq. (C.1) as “sum” divided by “diff”. Again neglecting radiative corrections, this expression becomes

$$\begin{aligned}
 A &= \frac{1}{2}(a + b)P_\mu \frac{F_{AS}}{F_{IS}} \\
 &= \frac{1}{2}(a + b)P_\mu \xi \times \\
 &\quad \frac{\frac{1}{3}\sqrt{x^2 - x_0^2} \left[ 1 - x + \frac{2}{3}\delta \left( 4x - 3 + \left( \sqrt{1 - x_0^2} - 1 \right) \right) \right]}{x(1 - x) + \frac{2}{9}\rho(4x^2 - 3x - x_0^2) + \eta x_0(1 - x)}
 \end{aligned}$$

The asymmetry at a particular momentum ( $x$ ) depends on all four of the Michel parameters, except at  $x = 0.75$ , where there is no sensitivity to  $\delta$  and  $\rho$ . The  $\rho$  and  $\delta$  dependences are very similar, and in the limit  $x_0 \rightarrow 0$ , the  $x$ -dependence of each parameter’s coefficients is  $(4x^2 - 3x)$ . This had implications for the pre-TWIST  $\delta$  result[113], which had to assume a value of  $\rho$  to extract  $\delta$  from the asymmetry. Also in the limit  $x \rightarrow 1$  (“the endpoint”), the asymmetry is proportional to  $P_\mu \xi \delta / \rho$ .

Integrating the asymmetry, with terms of order  $x_0^2$  neglected, Eq. (C.2) becomes

$$\begin{aligned}
 N_F(x) &= k_0(b - a)x \left\{ x(1 - x) + \frac{2}{9}\rho(4x^2 - 3x) + \eta x_0(1 - x) \right. \\
 &\quad \left. \pm \frac{1}{2}(b + a)\frac{1}{3}P_\mu \xi x \left[ 1 - x + \frac{2}{3}\delta(4x - 3) \right] \right\}, \tag{C.6}
 \end{aligned}$$

which shows the coefficients on  $\rho$  and  $\delta$  are  $(4x^3 - 3x^2)$ , and these integrate to 0 for a range of  $0 < x < 1$ . Therefore the integral asymmetry,  $(N_F - N_B)/(N_F + N_B)$ , depends on  $\xi$  and  $\eta$  only. If only a partial  $x$  range is integrated, then the asymmetry depends on all four muon decay parameters.

# Bibliography

- [1] Donald Hill Perkins. *Introduction to High-Energy Physics; 4th ed.* Cambridge Univ. Press, Cambridge, 2000.
- [2] C. Amsler et al. (Particle Data Group), 2008.
- [3] D. Griffiths. *Introduction to Elementary Particles.* Wiley, 1987.
- [4] M. Goldhaber, L. Grodzins, and A. W. Sunyar. Helicity of Neutrinos. *Phys. Rev.*, 109:1015 – 1017, 1958.
- [5] B. Jamieson. *Measurement of the muon decay asymmetry parameter with the TWIST spectrometer.* PhD thesis, University of British Columbia, 2006.
- [6] D. Binosi and L. Theußl. JaxoDraw: A graphical user interface for drawing Feynman diagrams. *Computer Physics Communications*, 161:76–86, August 2004.
- [7] C.A. Gagliardi, R.E. Tribble and N.J. Williams. Global analysis of muon decay measurements. *Phys. Rev. D*, 72, 2005.
- [8] W. Fetscher, H.-J. Gerber and K.F. Johnson. Muon decay: complete determination of the interaction and comparison with the standard model. *Physics Letters B*, 173(1):102–106, 1986.
- [9] R. P. MacDonald et al. Precision measurement of the muon decay parameters rho and delta. *Physical Review D (Particles and Fields)*, 78(3):032010, 2008.
- [10] W. Fetscher and H.-J. Gerber. Review of Particle Physics. *Phys. Lett. B*, 592, 2004.
- [11] A. B. Arbuzov. First-order radiative corrections to polarized muon decay spectrum. *Physics Letters B*, 524(1-2):99 – 106, 2002.
- [12] A. Czarnecki A. Arbuzov and A. Gaponenko. Muon decay spectrum: Leading logarithmic approximation. *Physical Review D*, 65:113006, 2002.

- [13] A. Arbuzov and K. Melnikov.  $\mathcal{O}(\alpha^2 \ln(m_\mu/m_e))$  corrections to electron energy spectrum in muon decay. *Physical Review D*, 66:093003, 2002.
- [14] A. Arbuzov. Higher order qed corrections to muon decay spectrum. *Journal of High Energy Physics*, 2003(03):063–063, 2003.
- [15] K. Melnikov C. Anastasiou and F. Petriello. The electron energy spectrum in muon decay through  $\mathcal{O}(\alpha^2)$ . *Journal of High Energy Physics*, (09):014, 2007.
- [16] R. MacDonald. *A Precision Measurement of the Muon Decay Parameters Rho and Delta*. PhD thesis, University of Alberta, 2008.
- [17] N. Danneberg et al. Muon Decay: Measurement of the Transverse Polarization of the Decay Positrons and its Implications for the Fermi Coupling Constant and Time Reversal Invariance. *Phys. Rev. Lett.*, 94:021802, 2005.
- [18] P. Herczeg. On muon decay in left-right-symmetric electroweak models. *Phys. Rev. D*, 34(11):3449–3456, Dec 1986.
- [19] V.M. Abazon et al. Search for W' Bosons Decaying to an Electron and a Neutrino with the D0 Detector. *Phys. Rev. Lett.*, 100:031804, 2008.
- [20] B. Jamieson et al. Measurement of  $p_\mu \xi$  in polarized muon decay. *Physical Review D (Particles and Fields)*, 74(7):072007, 2006.
- [21] S.P. Martin. A Supersymmetry Primer. Sep 1997. arXiv:hep-ph/9709356v5.
- [22] M. J. Ramsey-Musolf S. Profumo and S. Tulin. Supersymmetric contributions to weak decay correlation coefficients. *Physical Review D (Particles and Fields)*, 75(7):075017, 2007.
- [23] J.D. Jackson. *Classical Electrodynamics*. John Wiley & Sons, 1999.
- [24] V. Bargmann, L. Michel and V.L. Telegdi. Precession of the Polarization of Particles Moving in a Homogeneous Electromagnetic Field. *Phys. Rev. Lett.*, 2:435–436, 1959.
- [25] A. Balakin, V. Kurbanova and W. Zimdahl. Precession of a particle with anomalous magnetic moment in electromagnetic and gravitational pp-wave fields. *Gravity Cosmology Supplement*, 82:6–9, 2002.
- [26] P. Depommier. The BMT equation. Presentation to TWIST collaboration, May 2006.

- [27] P. Depommier. Muon depolarization in multiple scattering (TN100). Technical report, TRIUMF, 2005.
- [28] W.H. Koppenol. Names for muonium and hydrogen atoms and their ions(IUPAC Recommendations 2001). *Pure and Applied Chemistry*, 73:377–379, 2001.
- [29] M. Senba. Muon spin depolarization in noble gases during slowing down in a longitudinal magnetic field. *J. Phys. B: At. Mol. Opt. Phys.*, 31:5233–5260, 1998.
- [30] A. Jodidio et al. Search for right-handed currents in muon decay. *Physical Review D*, 34(7), 1986.
- [31] A. Jodidio et al. Erratum: Search for right-handed currents in muon decay. *Physical Review D*, 37(1), 1988.
- [32] J. H. Brewer. Muon spin rotation/relaxation/resonance. In *Encyclopedia of Applied Physics 11*, pages 23–53. 1994.
- [33] S.F.J. Cox. Implanted muon studies in condensed matter science. *J. Phys. C: Solid State Phys*, 20:3187–3319, 1987.
- [34] O. Hartmann et al. Diffusion of positive muons in some cubic metals. *Physics letters*, pages 141–142, 1977.
- [35] J. Brewer. Private communications.
- [36] W.B Gauster. Measurement of the depolarization rate of positive muons in copper and aluminum. *Solid State Communications*, pages 619–622, 1977.
- [37] W. Schilling. The physics of radiation damage in metals. *Hyperfine Interactions*, 4:636–644, 1978.
- [38] N. Haas et al. Muon trapping and diffusion in Al and In after electron irradiation at 9 K. *Hyperfine Interactions*, 31:217–222, 1986.
- [39] D.K. Brice. Lattice atom displacements produced near the end of implanted  $\mu^+$  tracks. *Phys. Lett. A*, 66:53–56, 1978.
- [40] P. Dalmas de Réotier and A. Yaouanc. Muon spin rotation and relaxation in magnetic materials. *J.Phys: Condens. Matter*, 9:9113–9166, 1997.

- [41] P. Dalmas de Réotier and A. Yaouanc. Quantum calculation of the muon depolarization function: effect of spin dynamics in nuclear dipole systems. *J.Phys: Condens. Matter*, 4:4533–4556, 1992.
- [42] A. Abragam. *Principles of Nuclear Magnetism*. International series of monographs on physics. Oxford University Press, 1986.
- [43] R.S. Hayano et al. Zero- and low-field spin relaxation studied by positive muons. *Phys. Rev. B*, 20:850, 1979.
- [44] W.J. Kossler et al. Diffusion and Trapping of Positive Muons in Al:Cu Alloys and in Deformed Al. *Physical Review Letters*, 41:1558–1561, 1978.
- [45] O. Hartmann et al. Coherent Propagation and Strain-Induced Localization of Muons in Al. *Physical Review Letters*, 41:1055–1058, 1978.
- [46] K.W. Kehr et al. Muon diffusion and trapping in aluminum and dilute aluminum alloys: Experiments and comparison with small-polaron theory. *Physical Review B*, 26:567–589, 1982.
- [47] K.W. Kehr. Empirical information on quantum diffusion. *Hyperfine Interactions*, 17-19:63–74, 1984.
- [48] O. Hartmann. Diffusion and trapping of muons in aluminum: New experiments and comparison with Kondo theory. *Physical Review B*, 37:4425–4440, 1988.
- [49] O. Hartmann. New results on diffusion in fcc metals. *Hyperfine Interactions*, 64:641–648, 1990.
- [50] O. Hartmann et al. Studies of  $\mu^+$  Localization in Cu, Al, and Al Alloys in the Temperature Interval 0.03 – 100 K. *Physical Review Letters*, 44:337–340, 1980.
- [51] D.P. Stoker et al. Search for Right-Handed Currents by Means of Muon Spin Rotation. *Physical review letters*, 54:1887–1890, 1985.
- [52] J. Korringa. Nuclear magnetic relaxation and resonance line shift in metals. *Physica*, 7-8:601–610, 1950.
- [53] S.J. Blundell and S.F.J. Cox. Longitudinal muon spin relaxation in metals and semimetals and the Korringa law. *J. Phys.: Condens. Matter*, 13:2163–2168, 2001.

- 
- [54] J.H. Brewer et al. *Positive muons and muonium in matter*. Muon Physics. Academic Press Inc (London) Limited, 1975.
- [55] S.F.J. Cox et al. Muon Korringa relaxation. *Physica B*, 289-290:594–597, 2000.
- [56] J.A. Brown et al. Muon Depolarization by Paramagnetic Impurities in Nonmagnetic Metals. *Physical Review Letters*, 47:261–264, 1981.
- [57] T.D. Lee and C.N. Yang. Question of Parity Conservation in Weak Interactions. *Physical Review*, 104:254, October 1956.
- [58] ARGUS collaboration. Determination of the Michel Parameters  $\rho$ ,  $\xi$ , and  $\delta$  in  $\tau$ -Lepton Decays with  $\tau \rightarrow \rho\nu$  Tags. *Physics Letters B*, 431:179–187, 1998.
- [59] L3 Collaboration. Measurement of the Michel parameters and the average tau-neutrino helicity from tau decays at LEP. *Physics Letters B*, 438:405–416, 1998.
- [60] R. Bartoldus. Measurements of the Michel Parameters in Leptonic Tau Decays using the OPAL Detector at LEP. *Nuclear Physics B (Proc. Suppl.)*, 76:147–157, 1999.
- [61] R.L. Garwin, L.M. Lederman and M. Weinrich. Observations of the Failure of Conservation of Parity and Charge Conjugation in Meson Decays: the Magnetic Moment of the Free Muon. *Physical Review*, 105:1415, January 1957.
- [62] G. R. Lynch, J. Orear, and S. Rosendorff. Muon decay in nuclear emulsion at 25 000 gauss. *Phys. Rev.*, 120(6):2277, Dec 1960.
- [63] Ali-Zade et al. *Soviet Phys.-JETP*, 36 (9):940, 1959.
- [64] M. Bardon, D. Berley, and L. M. Lederman. Asymmetry parameter in muon decay. *Phys. Rev. Lett.*, 2(2):56–57, Jan 1959.
- [65] Richard J. Plano. Momentum and asymmetry spectrum of  $\mu$ -meson decay. *Phys. Rev.*, 119(4):1400–1408, Aug 1960.
- [66] Akhmanov et al. *Sov. J. Nucl. Phys*, 6:230, 1968.
- [67] I. Beltrami et al. Muon decay: Measurement of the integral asymmetry parameter. *Physics Letters B*, 194(2):326–330, 1987.
- [68] R.S. Hayano et al. Search for right-handed currents in the decay  $k^+ \rightarrow \mu^+\nu$ . *Phys. Rev. Lett.*, 52(5):329–332, Jan 1984.

- [69] J. Imazato et al. Search for right-handed currents in the decay chain  $k^+ \rightarrow \mu^+\nu$ ,  $\mu^+ \rightarrow e + \nu\bar{\nu}$ . *Phys. Rev. Lett.*, 69(6):877–880, Aug 1992.
- [70] T. Yamanaka et al. Search for right-handed currents in the decay  $k^+ \rightarrow \mu^+\nu$ . *Phys. Rev. D*, 34(1):85–96, Jul 1986.
- [71] C.A. Coombes et al. Polarization of  $\mu^+$  mesons from the decay of  $k^+$  mesons.
- [72] D. Cutts, T. Elioff, and R. Stiening. Muon polarization and energy spectrum in  $k^+ \rightarrow \pi^0 + \mu^+ + \nu$ . *Phys. Rev.*, 138(4B):B969–B979, May 1965.
- [73] D. Cutts, R. Stiening, C. Wiegand, and M. Deutsch. Measurement of the muon polarization vector in  $k^+ \rightarrow \pi^0 + \mu^+ + \nu$ . *Phys. Rev.*, 184(5):1380–1392, Aug 1969.
- [74] R.S. Henderson et al. Precision planar drift chambers and cradle for the TWIST muon decay spectrometer. *Nuclear Instruments and Methods in Physics Research Section A*, 548:306–335, August 2005.
- [75] J. Hu et al. Time expansion chamber system for characterization of TWIST low-energy muon beams. *Nuclear Instruments and Methods in Physics Research Section A*, 566:563–574, October 2006.
- [76] C.J. Oram, J.B. Warren and G.M. Marshall. Commissioning of a new low energy  $\pi - \mu$  channel at TRIUMF. *Nuclear Instruments and Methods*, 179:95–103, January 1981.
- [77] J. Doornbos. The tuning of M13 for TWIST, theory and some results. Posted to TWIST bulletin boards, December 2000.
- [78] N. Rodning. TWIST: Precision Muon Decay at TRIUMF. Submitted to NSERC in support of grant application., 2000.
- [79] O.B. van Dyck et al. 'Cloud' and 'Surface' muon beam characteristics. *IEEE Transactions on Nuclear Science*, NS-26, June 1979.
- [80] G.M. Marshall. Private communications.
- [81] T. Prokscha et al. The new  $\mu$ E4 beam at PSI: A hybrid-type large acceptance channel for the generation of a high intensity surface-muon beam. *Nuclear Instruments and Methods in Physics Research A*, 595.
- [82] J.E. Draper. Beam Steering with Quadrupole and with Rectangular Box Magnets. *Rev. Sci. Instrum.*, 37:1390, October 1966.

- [83] J. Musser. *Measurement of the Michel parameter  $\rho$  in muon decay*. PhD thesis, Texas A&M University, 2005.
- [84] Vector Fields. OPERA 3D simulation software. <http://vectorfields.com>.
- [85] A. Gaponenko. *A Precision Measurement of the Muon Decay Parameter Delta*. PhD thesis, University of Alberta, 2005.
- [86] D. Wright. TN1: DME / He WC Gas Comparison. Technical report, TRIUMF, October 1996.
- [87] LeCroy Corporation. 1877 Multihit Time-to-Digital Converter: Specification. Internet webpage.
- [88] LeCroy Corporation. LeCroy 1877 Fastbus TDC Manual. Hosted by TRIUMF DAQ group.
- [89] R. Veenhof. Garfield - simulation of gaseous detectors. <http://garfield.web.cern.ch>.
- [90] R. Brun and F. Rademakers. ROOT - An Object Oriented Data Analysis Framework. *Nucl. Inst. & Meth. in Phys. Res. A*, 389:81–86, 1997.
- [91] F. James. Fitting tracks in wire chambers using the Chebyshev Norm instead of least squares. *Nuclear Instruments and Methods*, 211:145–152, 1983.
- [92] R. Bayes. *Measurement of  $\rho$* . PhD thesis, University of Victoria, 2009.
- [93] C. Gagliardi. Private communications.
- [94] P. Depommier. TN49: Muon polarisation in electromagnetic fields. Technical report, TRIUMF, 2001.
- [95] S.R. Dunsiger et al. Magnetic field dependence of muon spin relaxation in geometrically frustrated  $\text{Gd}_2\text{Ti}_2\text{O}_7$ . *Physical Review B*, 73(172418), 2006.
- [96] J. L. Beveridge et al. A spin rotator for surface  $\mu^+$  beams on the new m20 muon channel at triumph. *Nuclear Instruments and Methods in Physics Research Section A*, 240:316–322, 1985.
- [97] Triumph CMMS. Helios superconducting solenoid. Website: <http://cmms.triumf.ca/equip/helios.html>.

- [98] J.F. Ziegler. The stopping and range of ions in matter. <http://www.srim.org/>.
- [99] TRIUMF CS. TRIUMF Computing Services description of SRIM. <http://it-services.triumf.ca/scientific-computing/software/detector-engineering/srim-1>.
- [100] D.M. Garner. *Application of the muonium spin rotation technique to a study of the gas phase chemical kinetic of muonium reactions with the halogens and hydrogen halides*. PhD thesis, University of British Columbia, June 1979.
- [101] R. Barlow. Systematic errors: facts and fictions. *arXiv:hep-ex/0207026*, 2002.
- [102] H. Yukawa. On the Interaction of Elementary Particles. *I, Proc. Phys.-Math. Soc. Jpn.*, 17:48, 1935.
- [103] C.D. Anderson and S.H. Neddermeyer. Cloud Chamber Observations of Cosmic Rays at 4300 Meters Elevation and Near Sea-Level. *Phys. Rev.*, 50:263–271, 1936.
- [104] S.H. Neddermeyer and C.D. Anderson. Cosmic-Ray Particles of Intermediate Mass. *Phys. Rev.*, 54:88–89, 1938.
- [105] S.H. Neddermeyer and C.D. Anderson. Nature of Cosmic-Ray Particles. *Rev. Mod. Phys.*, 11:191–207, 1939.
- [106] M. Riordan. *The Hunting of the Quark*. Sage Publications, 1987.
- [107] M. Conversi, E. Pancini and O. Piccioni. On the Disintegration of Negative Mesons. *Phys. Rev.*, 71:209–210, 1947.
- [108] E. Fermi, E. Teller and V. Weisskopf. The Decay of Negative Mesotrons in Matter. *Phys. Rev.*, 71:314–315, 1947.
- [109] C.M.G. Lattes, G.P.S. Occhialini and C.F. Powell. Observations on the Tracks of Slow Mesons in Photographic Emulsions Part 1. *Nature*, 160:453–456, 1947.
- [110] C.M.G. Lattes, G.P.S. Occhialini and C.F. Powell. Observations on the Tracks of Slow Mesons in Photographic Emulsions Part 1. *Nature*, 160:486–492, 1947.
- [111] C.S. Wu and V.W. Hughes. *Muon Physics: Introduction and History*. Academic Press Inc., 1977.
- [112] T.D. Lee. A Brief History of the Muon. *Hyperfine Interactions*, 86:439–453, 1994.

[113] B. Balke et al. Precise measurement of the asymmetry parameter  $\delta$  in muon decay.  
*Physical Review D*, 37:587–617, 1988.

[114] J. Doornbos. Private communications.